ACS Catalysis

pubs.acs.org/acscatalysis Letter

Planar Chiral 1,3-Disubstituted Ferrocenyl Phosphine Gold(I) Catalysts

Ulysse Caniparoli, Imma Escofet, and Antonio M. Echavarren*

Cite This: ACS Catal. 2022, 12, 3317−3322 Read Online

ACCESS | Metrics & More | Article Recommendations | Supporting Information

ABSTRACT: Planar chiral monodentate 1,3-disubstituted ferrocene phosphines inspired on JohnPhos-type ligands have been synthesized and applied to the enantioselective gold(I) catalyzed [4 + 2] cycloaddition of 1,6-arylenynes. Computational studies rationalized the working mode of the catalyst on the folding of the substrate in the chiral environment of the ligand involving attractive noncovalent interactions.

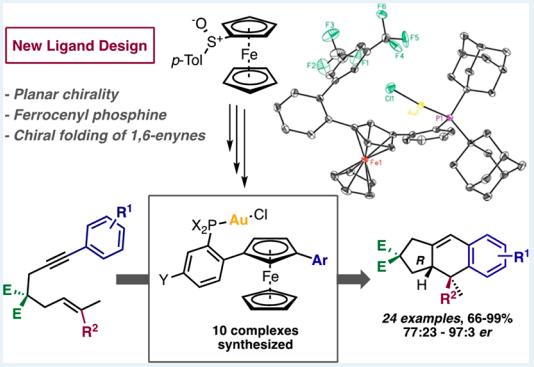

KEYWORDS: *gold catalysis, planar chirality, ferrocene phosphines, enantioselective synthesis, enynes, DFT calculations*

In the wake of the first introduction of chiral ferrocene-based ligands by Hayashi for the asymmetric rhodium-catalyzed hydrosilylation of ketones,[1] ferrocenyl phosphines have became one of the most versatile scaffolds in chiral ligand design. Since the pioneering work of Ugi,[2] followed by those of Kagan,[3] Richard,[4] Uemura,[5] and Sammakia,[6] C_2-functionalization of enantiopure ferrocenes by a chiral directing metalation group allowed the access of a variety of chiral 1,2-disubstituted ferrocene ligands such as PPFA,[1] Josiphos,[7] Fcphox,[4] and Fesulphos,[8] among others.[9] Ferrocenyl phosphine ligands are mainly bidentate and display central chirality in addition to planar chirality, which plays a crucial role on the enantioinduction.[10] The pioneering examples in enantioselective gold(I) catalysis[11] referred to the use of a chiral ferrocenyl phosphine-gold(I) catalysts in the asymmetric aldol reaction between aldehydes and isocyanoacetates.[12] Since then, very few examples have been reported in gold(I) asymmetric catalysis using this type of complex.[13] Our group found that digold(I) complexes with 1,2-disubstituted ferrocenyl ligands of the Josiphos family were the most efficient catalysts for the first enantioselective intermolecular gold(I)-catalyzed [2 + 2] cycloaddition of terminal alkynes and alkenes.[14]

In sharp contrast to the synthesis of 1,2-disubstituted ferrocenes, the enantioselective syntheses of 1,3-disubstituted scaffolds are still scarce,[15] even if these structures appear to be promising for different applications.[16] Therefore, we focused our efforts on the synthesis of ferrocene phosphine ligands displaying exclusively planar chirality, thus eliminating the possibility of match-mismatch cases and facilitating investigations on the mode of action of the new catalysts. We have recently achieved a high level of enantioselectivity in asymmetric gold(I) catalysis using a chiral JohnPhos-type gold(I) complex **1** with a C_2-symmetric pyrrolidine.[17] We envisioned that the planar chirality of a 1,3-disubstitued ferrocene could provide a somewhat similar chiral environment to that of the C_2-symmetric pyrrolidine, while maintaining the bulky dialkylphosphine that is characteristic of JohnPhos ligands in order to direct the substrate coordinated to gold(I) toward the ferrocene scaffold and the chiral reaction scenario, where the enantiodiscrimination takes place (Scheme 1). Here, we report the synthesis of new 1,3-disubstituted ferrocene ligands and their application to the gold(I)-catalyzed intramolecular formal [4 + 2] cyclization of arylalkynes to alkenes, which takes place with consistently high enantioselectivities.

The readily available enantiopure chiral ferrocenyl sulfoxide **2**[18] was used as the starting material in our synthetic route (Scheme 2). The preparation of the new ligands commenced by diastereoselective lithiation of **2** with LDA, followed by addition of $ZnCl_2$ and Negishi cross-coupling yielding planar chiral ferrocenes **4a−f**. For the second directed *ortho*-lithiation the configuration of the sulfoxide had to be inverted by a reduction−oxidation[19] sequence yielding sulfoxides **5a-f**. After

Received: December 17, 2021
Revised: February 15, 2022
Published: February 25, 2022

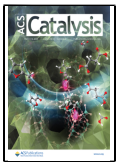

https://doi.org/10.1021/acscatal.1c05827
ACS Catal. 2022, 12, 3317−3322

Scheme 1. Design of Chiral Monodentate Ferrocene-Based Ligands

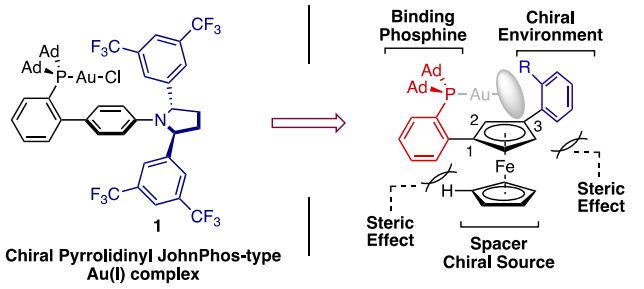

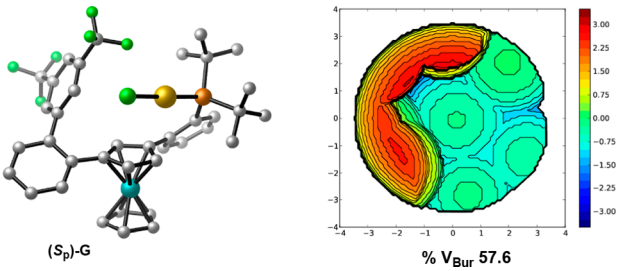

Figure 1. CYLview depiction of the X-ray crystal structure of ferrocenyl gold(I) complex (S_p)-**G** and steric maps by SamVca 2.1. Hydrogen atoms are omitted for clarity.

ortho-lithiation of sulfoxides **5** with LiTMP and reaction with Bu_3SnCl, the sulfoxide group was removed by reaction with *t*BuLi and protonolysis with *i*PrOH.[15a] The resulting tributylstannyl-ferrocenes underwent Sn−Li exchange with *n*BuLi, followed by addition of $ZnCl_2$, Negishi coupling with 2-bromo-1-iodoarenes, and palladium-catalyzed coupling reaction with phosphines X_2PH giving rise to ligands $\mathbf{6}_{A-I}$, which afforded the corresponding gold(I)-complexes **A**−**I** by addition of Me_2S·AuCl. Complexes **A** and **C**−**F** were directly obtained without isolation of the corresponding ligands **6**. The structure of complexes **A**−**C**, **G**, and **H** was confirmed by X-ray diffraction.

The crystallographic Au−P distance 2.293 Å found for (S_p)-**G** is essentially identical to that determined for the chiral JohnPhos-type gold(I) complex **1**.[17] The buried volume for (S_p)-**G** was calculated using SambVca 2.1 (Figure 1).[20] As revealed by the steric profile, the aromatic biphenyl substituents on the ferrocenyl moiety provide rather significant hindrance to the complex with a buried volume of 57.6%. As a comparison, buried volumes of [(PR_3)AuCl] complexes with R = *t*Bu, *o*Tol, and Mes are 38.1, 39.4, and 45.0%, respectively (2.28 Å, Au−P length).[21] Buried volumes of 45−53% have been reported for other gold(I) complexes bearing bulky alkoxydiaminophosphine[22] or acyclic diaminocarbene ligands.[23]

To compare the reactivity of the new ferrocenyl phosphine gold(I) complexes with that of **1**,[17] we studied the [4 + 2] cycloaddition of 1,6-arylenynes **7** (Scheme 3). First, we studied the reaction of substrate **7n** with **A**−**I** complexes (Table 1). Among the tested silver(I) salts, the best results were obtained with $AgBF_4$.[24] The highest enantioselectivity was obtained with complexes **A**, **B**, and **H** with two adamanthyl groups at the phosphine, which yielded cycloadduct **8n** in 87−89:11−13 er (Table 1, entries 1−2 and 15). Complexes **C**−**E** and **G** led to lower enantioselectivities (Table 1, entries 10−12 and 14), whereas nearly racemic mixtures were obtained with **F** and **I** with two aryl groups at the phosphine (Table 1, entries 13 and 16). Although complex **B** provided **8n** with higher enantioselectivity in toluene than in $(CH_2Cl)_2$ at 24 °C (88:12 vs 83:17 er) (Table 1, entries 3 and 7), at −25 °C no conversion of **7n** was observed in toluene (Table 1, entries 4 and 8). In general, less clean conversions were observed in toluene or other aromatic solvents (Table 1, entries 5−6 and 9). A related complex with a 1-napthlyl group at C-3 of the ferrocene was also prepared,[24] although product **8a** was obtained in poor enantiomeric ratios (75%, 57:43 er).

Complex **B**, conveniently prepared from ferrocenyl sulfoxide **2** in 48% overall yield in a 0.8 mmol scale, was selected for practical purposes (Scheme 3). 1,6-Enynes **7a**−**b** yielded cycloadducts **8a**−**b** in moderate enantioselectivities, while enyne **7c** with a tether with two methoxymethyl groups

Scheme 2. Synthesis of Gold(I) Complexes A−I from Ferrocenyl Sulfoxide (S_S)-2

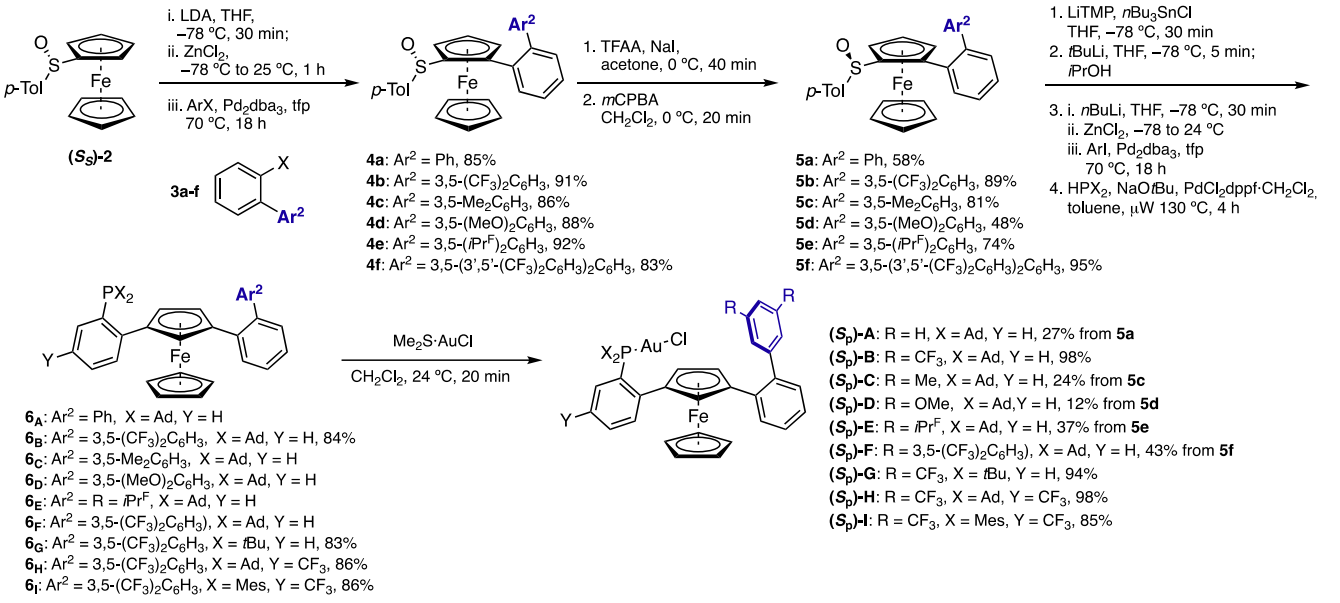

4a: Ar^2 = Ph, 85%
4b: Ar^2 = 3,5-$(CF_3)_2C_6H_3$, 91%
4c: Ar^2 = 3,5-$Me_2C_6H_3$, 86%
4d: Ar^2 = 3,5-$(MeO)_2C_6H_3$, 88%
4e: Ar^2 = 3,5-$(iPr^F)_2C_6H_3$, 92%
4f: Ar^2 = 3,5-(3',5'-$(CF_3)_2C_6H_3)_2C_6H_3$, 83%

5a: Ar^2 = Ph, 58%
5b: Ar^2 = 3,5-$(CF_3)_2C_6H_3$, 89%
5c: Ar^2 = 3,5-$Me_2C_6H_3$, 81%
5d: Ar^2 = 3,5-$(MeO)_2C_6H_3$, 48%
5e: Ar^2 = 3,5-$(iPr^F)_2C_6H_3$, 74%
5f: Ar^2 = 3,5-(3',5'-$(CF_3)_2C_6H_3)_2C_6H_3$, 95%

6_A: Ar^2 = Ph, X = Ad, Y = H
6_B: Ar^2 = 3,5-$(CF_3)_2C_6H_3$, X = Ad, Y = H, 84%
6_C: Ar^2 = 3,5-$Me_2C_6H_3$, X = Ad, Y = H
6_D: Ar^2 = 3,5-$(MeO)_2C_6H_3$, X = Ad, Y = H
6_E: Ar^2 = R = iPr^F, X = Ad, Y = H
6_F: Ar^2 = 3,5-$(CF_3)_2C_6H_3$), X = Ad, Y = H
6_G: Ar^2 = 3,5-$(CF_3)_2C_6H_3$, X = *t*Bu, Y = H, 83%
6_H: Ar^2 = 3,5-$(CF_3)_2C_6H_3$, X = Ad, Y = CF_3, 86%
6_I: Ar^2 = 3,5-$(CF_3)_2C_6H_3$, X = Mes, Y = CF_3, 86%

(S_p)-**A**: R = H, X = Ad, Y = H, 27% from **5a**
(S_p)-**B**: R = CF_3, X = Ad, Y = H, 98%
(S_p)-**C**: R = Me, X = Ad, Y = H, 24% from **5c**
(S_p)-**D**: R = OMe, X = Ad,Y = H, 12% from **5d**
(S_p)-**E**: R = iPr^F, X = Ad, Y = H, 37% from **5e**
(S_p)-**F**: R = 3,5-$(CF_3)_2C_6H_3$), X = Ad, Y = H, 43% from **5f**
(S_p)-**G**: R = CF_3, X = *t*Bu, Y = H, 94%
(S_p)-**H**: R = CF_3, X = Ad, Y = CF_3, 98%
(S_p)-**I**: R = CF_3, X = Mes, Y = CF_3, 85%

https://doi.org/10.1021/acscatal.1c05827
ACS Catal. 2022, 12, 3317−3322

Scheme 3. Enantioselective Gold(I)-Catalyzed [4 + 2] Cycloaddition of 1,6-Arylenynes 7a−x with Catalyst B

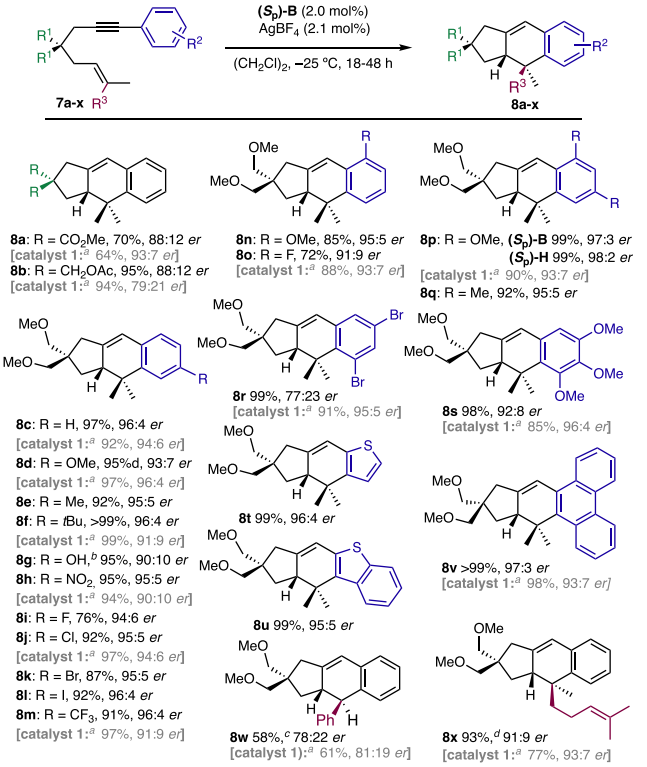

[a]Previously reported reactions performed using catalyst **1** (4 mol %), $AgPF_6$ (4 mol %), and at 24 °C.[17] [b]Reaction performed at −10 °C. [c]Reaction time = 12 days (vs 14 days with **1**). [d]Reaction time = 6 days (vs 7 days with **1**).

Table 1. Optimization of the Enantioselective Gold(I)-Catalyzed [4 + 2] Cycloaddition of 1-6-Arylenyne 7n

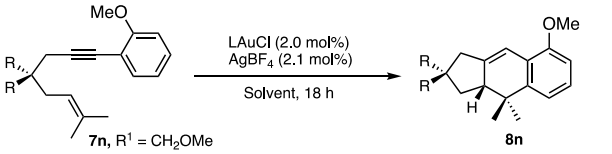

entry	complex	solvent	T (°C)	yield (%)[b]	er[c]
1	(S_p)-**A**	$(CH_2Cl)_2$	0	88	87:13
2	(S_p)-**B**	$(CH_2Cl)_2$	0	95	88:12
3	(S_p)-**B**	$(CH_2Cl)_2$	24	92	83:17
4	(S_p)-**B**	$(CH_2Cl)_2$	−25	81[d]	94:6
5	(S_p)-**B**	CH_2Cl_2	24	90	85:15
6	(S_p)-**B**	CH_2Cl_2	−25	82[f]	95:5
7	(S_p)-**B**	toluene	24	75[g]	88:12
8	(S_p)-**B**	toluene	−25	nd.[h]	-
9	(S_p)-**B**	$PhCF_3$	24	77	86:14
10	(S_p)-**C**	$(CH_2Cl)_2$	0	95	82:18
11	(S_p)-**D**	$(CH_2Cl)_2$	0	89	74:26
12	(S_p)-**E**	$(CH_2Cl)_2$	0	95	73:27
13	(S_p)-**F**	$(CH_2Cl)_2$	0	89	56:44
14	(S_p)-**G**	$(CH_2Cl)_2$	0	93	85:15
15	(S_p)-**H**	$(CH_2Cl)_2$	0	92	89:11
16	(S_p)-**I**	$(CH_2Cl)_2$	0	89[e]	49:51

[a]0.06 mmol scale. [b]Yield determined by ^{1}H NMR using 1,1,2-trichloroethane as internal standard. [c]er determined by chiral-SFC apparatus. [d](91 brsm). [e]Reaction performed over 96 h. [f]Reaction performed for 24 h. [g]Reaction performed for 5 days. [h]No detection.

afforded product **8c** in excellent yield and enantioselectivity. Substrates **7d−o** with bulky, electron-donating or electron-withdrawing groups in *para*- and *ortho*-positions of the aryl ring underwent [4 + 2] cycloaddition in high to excellent yields and enantiomeric ratios. The cyclization of 1,6-enyne **7g** with a free phenol was carried out at −10 °C, as this substrate is insoluble in $(CH_2Cl)_2$ at −25 °C, and yielded product **8g** with good enantioselectivity. 2,4-Disubstituted arylenynes **7p** and **7q** reacted smoothly delivering respectively products **8p** and **8q** in good yield and high enantiomeric ratio. Using complex **H** as the catalyst, substrate **7p** led to **8p** almost quantitatively in 98:2 er.

Lower enantioselectivity was obtained with 3,5-dibromophenyl-substituted 1,6-arylenyne **7r**, which gave product **8r** quantitatively but only in 77:23 er, while trimethoxy substituted arylenyne **7s** gave **8s** in 92:8 er. Phenanthrene-substituted enyne **7v** delivered product **8v** in excellent yield and enantioselectivity. Sulfur-containing heterocycles **7t** and **7u**, respectively bearing thiophene and benzothiophene moieties, also reacted smoothly, affording the corresponding products **8t** and **8u** in high yields and good enantiomeric ratios. In general, the intramolecular [4 + 2] cycloadditions were completed in 18−48 h at −25 °C with ferrocenyl phosphine gold(I) complex (S_p)-**B**, whereas reactions with complex **1** had to be performed at 24 °C. Previous results obtained with catalyst **1**[17] are also included in Scheme 3. Comparison of the rate of formation of **8c** from enyne **7c** using gold(I) complexes **B** and **1** in the presence of $AgBF_4$ or $AgPF_6$ showed **B** the significantly more reactive.[24] On the other hand, reactions leading to **8w** and **8x** were very slow with both catalysts **B** and **1**. Performing reaction of **7w** at 25 °C with catalyst **B** afforded **8w** in 65% yield after in 84 h but only with 66:34 er. The absolute configuration of products **8** were assigned by comparison with previously reported results.[17]

To better rationalize the working mode of these novel ferrocenyl-based phosphine gold(I) complexes, we carried out DFT calculations.[24] We started our investigations computing the reaction coordinate for the cyclization of enyne **7c** (Figure 2a). BP86-D3 has been chosen as a functional due to is efficiency proved in other studies of enantioselective gold(I) catalysis,[14,17,25] and in our recent benchmark of DFT functionals using similar systems.[26] We used (S_p)-**G** as gold(I) catalyst (bearing *t*Bu substituted phosphine), which is similar but simpler than (S_p)-**B**. Our calculations herein center on the intramolecular electrophilic addition of $[LAu(\eta^2\text{-alkyne})]^+$ complex to the alkene ($\mathbf{Int_{1a-b}}$ to $\mathbf{Int_{2a-b}}$), as the enantiodetermining step of the transformation. We calculated two possible minima resulting from the reaction of the two enantiotopic faces of the alkene (*R* and *S* pathways) and examined the evolution of the two possible gold(I)-complexes $\mathbf{Int_{1a-b}}$ following an exocyclic pathway. The calculated energy difference between the lowest transition states that lead to **Int2a** and **Int2b** $\Delta G^{\ddagger}_{R\text{-}S}$ = 1.2 kcal/mol are in good agreement with the experimental results (96:4 er). The lowest transition state $\mathbf{TS_{Int1-2a}}$ was found to be stabilized by $\pi-\pi$-interactions[27] and the lack thereof in $\mathbf{TS_{Int1-2b}}$. Therefore, cyclopropyl gold(I) carbene **Int2a** with the *R* absolute configuration is preferentially formed. We further examined the attractive interactions between the π-systems of the substrate and the catalyst. Hence, larger green surfaces were observed in the NCI plots[28] of the lowest-energy transition state $\mathbf{TS_{Int1-2a}}$ in comparison to $\mathbf{TS_{Int1-2b}}$, confirming that noncovalent inter-

https://doi.org/10.1021/acscatal.1c05827
ACS Catal. 2022, 12, 3317−3322

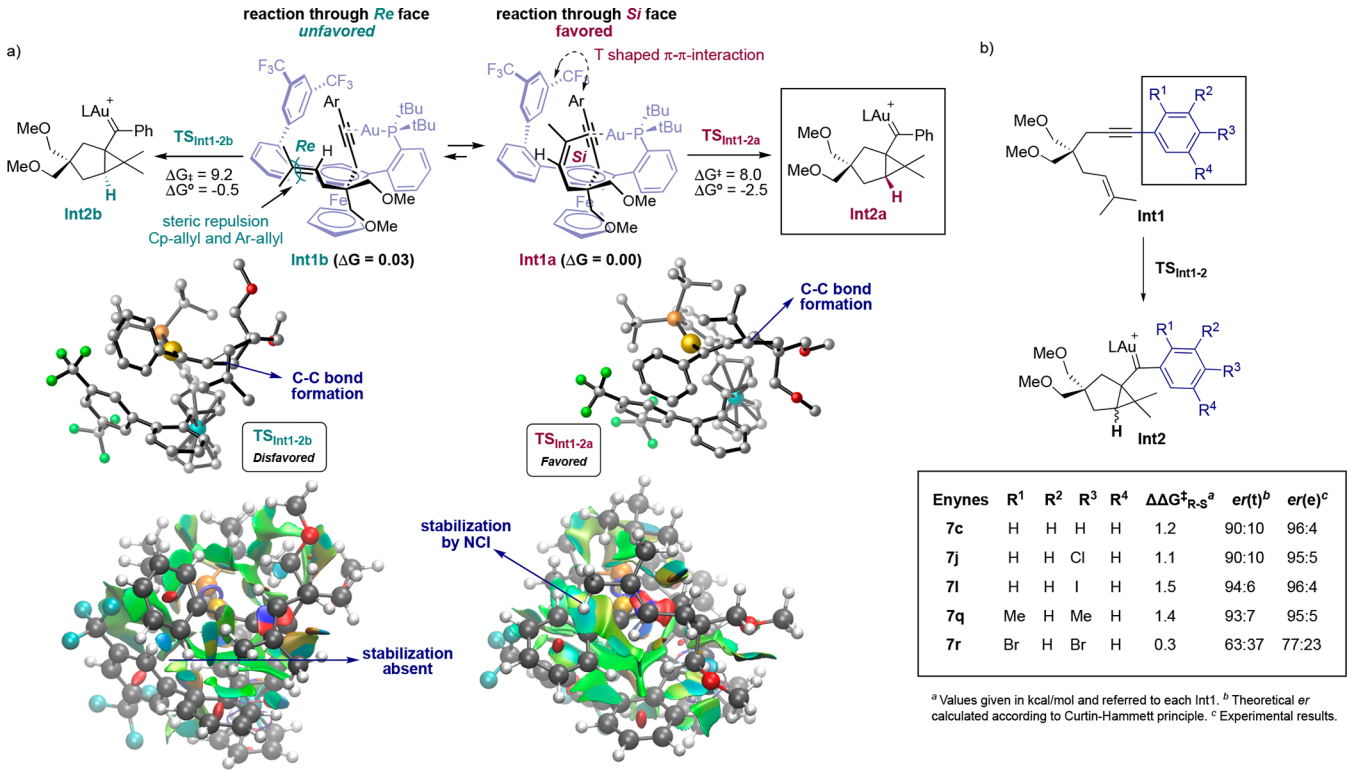

Enynes	R^1	R^2	R^3	R^4	$\Delta\Delta G^{\ddagger}_{R\text{-}S}$[a]	er(t)[b]	er(e)[c]
7c	H	H	H	H	1.2	90:10	96:4
7j	H	H	Cl	H	1.1	90:10	95:5
7l	H	H	I	H	1.5	94:6	96:4
7q	Me	H	Me	H	1.4	93:7	95:5
7r	Br	H	Br	H	0.3	63:37	77:23

[a] Values given in kcal/mol and referred to each Int1. [b] Theoretical *er* calculated according to Curtin-Hammett principle. [c] Experimental results.

Figure 2. (a) Free-energy profile for the gold(I)-catalyzed cyclization of 1,6-enyne **7c** with (S_p)-**G**. *S*-pathways are depicted in green and *R*-pathways in purple (energies in kcal/mol). CYLview representations and NCI plots of the two possible transition states **TSInt1−2a** and **TSInt1−2b**. Hydrogens are omitted for clarity. Color-filled RDG isosurface. Blue color: strong attractive interactions (C−C bond formation), green color: attractive noncovalent interactions, red color: areas of repulsion (steric and ring effects). (b) Calculation of difference in activation energies ($\Delta\Delta G^{\ddagger}_{R\text{-}S}$) between *R* and *S* enantiomers in different substrates.

actions play a fundamental role in the stabilization of the corresponding transition states.

Although this theoretical study provided a model to explain the preferred formation of *R*-enantiomer of **8c**, we further examined this system by changing the aromatic ring substituents on the substrates (R1−4 in **Int1**) to better understand the limitations of our catalysts (Figure 2b).[24] Thus, we computationally studied enynes **7j**, **7l**, **7q**, **7r** using the same (S_p)-**G** gold complex. For *para*-substituted aryl enynes **7j** and **7l**, the activation energies to reach **Int2a** was lower by at least 1.1 kcal/mol than the alternative pathway that gives rise to **Int2b** in both cases, in agreement with the experimental results (95:5 er for product **8j** and 96:4 er for **8l**). Interestingly, both cyclopropyl gold carbenes **Int2a** of enynes **7j** and **7l** were found to be more stable than the other examples due to the conformation adopted in the chiral pocket.[24] Having a methyl group in *ortho*- and *para*-position of the aryl ring of enyne **7q** was crucial to achieve higher enantioselectivity ($\Delta\Delta G^{\ddagger}_{R\text{-}S}$ = 1.4 kcal/mol). However, very similar activation energies were found for the two competing pathways of the 3,5-dibromophenyl-substituted 1,6-arylenyne **7r**. Thus, in this case, formation of **Int2a** was favored by only 0.3 kcal/mol, in good agreement with the lower enantiomeric ratio obtained experimentally (77:23 er). This drop of enantioselectivity can be rationalized by the lower noncovalent interactions in the transition state as well as the steric repulsion due to the bulkiness of the bromine forcing the substrate away from the chiral environment of the catalyst.[24]

In summary, we have synthesized unprecedented gold(I) complexes with planar chiral monodentate ferrocene-based ligands by iterative *ortho*-lithiation/transmetalation/Negishi cross-coupling reactions and palladium-catalyzed phosphine cross-coupling. This is the first synthetic route leading to planar chiral analogues of the JohnPhos-type ligands. The new chiral 1-(2′-dialkylarylphosphine)-3-arylferrocene gold(I) complexes allow performing the formal intramolecular [4 + 2] cycloaddition of arylalkynes with alkenes with high enantioselectivities and with higher reactivity than our recently reported JohnPhos-type gold(I) complexes with a C_2-symmetric pyrrolidine.[17] Computational studies provide a working model showing a very good agreement with the experimental results, which indicates that noncovalent $\pi-\pi$-interactions between substrates and the ligand are responsible of the selective folding of substrates in the chiral environment of the gold(I) catalyst.

■ ASSOCIATED CONTENT

Supporting Information

The Supporting Information is available free of charge at https://pubs.acs.org/doi/10.1021/acscatal.1c05827.

Experimental procedures, characterization data, NMR data, UPC2 and HPLC traces, computational details, and X-ray data (PDF)

Accession Codes

CCDC 2129524−2129528 contain the supplementary crystallographic data for this paper. These data can be obtained free of charge via www.ccdc.cam.ac.uk/data_request/cif, or by emailing data_request@ccdc.cam.ac.uk, or by contacting The Cambridge Crystallographic Data Centre, 12 Union Road, Cambridge CB2 1EZ, UK; fax: + 44 1223 336033.

https://doi.org/10.1021/acscatal.1c05827
ACS Catal. 2022, 12, 3317−3322

AUTHOR INFORMATION

Corresponding Author

Antonio M. Echavarren − *Institute of Chemical Research of Catalonia (ICIQ), Barcelona Institute of Science and Technology, 43007 Tarragona, Spain; Departament de Química Analítica i Química Orgànica, Universitat Rovira i Virgili, 43007 Tarragona, Spain;* orcid.org/0000-0001-6808-3007; Email: aechavarren@iciq.es

Authors

Ulysse Caniparoli − *Institute of Chemical Research of Catalonia (ICIQ), Barcelona Institute of Science and Technology, 43007 Tarragona, Spain; Departament de Química Analítica i Química Orgànica, Universitat Rovira i Virgili, 43007 Tarragona, Spain*

Imma Escofet − *Institute of Chemical Research of Catalonia (ICIQ), Barcelona Institute of Science and Technology, 43007 Tarragona, Spain; Departament de Química Analítica i Química Orgànica, Universitat Rovira i Virgili, 43007 Tarragona, Spain*

Complete contact information is available at: https://pubs.acs.org/10.1021/acscatal.1c05827

Notes

The authors declare no competing financial interest.

ACKNOWLEDGMENTS

We thank the MCIN/AEI/10.13039/501100011033 (PID2019-104815GB-I00 and CEX2019-000925-S), the European Research Council (Advanced Grant 835080), the AGAUR (2017 SGR 1257), and the CERCA Program/Generalitat de Catalunya for financial support. We also thank the ICIQ X-ray diffraction unit. We thank Àlex Martí and Isabel Arranz for help in the preparation of some starting materials.

REFERENCES

(1) Hayashi, T.; Yamamoto, K.; Kumada, M. Asymmetric Catalytic Hydrosilylation of Ketones Preparation of Chiral Ferrocenylphosphines as Chiral Ligands. *Tetrahedron Lett.* **1974**, *15*, 4405−4408.

(2) Marquarding, D.; Klusacek, H.; Gokel, G.; Hoffmann, P.; Ugi, I. Correlation of Central and Planar Chirality in Ferrocene Derivatives. *J. Am. Chem. Soc.* **1970**, *92*, 5389−5393.

(3) (a) Riant, O.; Samuel, O.; Kagan, H. B. A General Asymmetric Synthesis of Ferrocenes with Planar Chirality. *J. Am. Chem. Soc.* **1993**, *115*, 5835−5836. (b) Guillaneux, D.; Kagan, H. B. High Yield Synthesis of Monosubstituted Ferrocenes. *J. Org. Chem.* **1995**, *60*, 2502−2505.

(4) Richards, C. J.; Damalidis, T.; Hibbs, D. E.; Hursthouse, M. B. Synthesis of 2-[2-(Diphenylphosphino)Ferrocenyl]Oxazoline Ligands. *Synlett* **1995**, *1995*, 74−76.

(5) Nishibayashi, Y.; Segawa, K.; Ohe, K.; Uemura, S. Chiral Oxazolinylferrocene-Phosphine Hybrid Ligand for the Asymmetric Hydrosilylation of Ketones. *Organometallics* **1995**, *14*, 5486−5487.

(6) Sammakia, T.; Latham, H. A.; Schaad, D. R. Highly Diastereoselective Ortho Lithiations of Chiral Oxazoline-Substituted Ferrocenes. *J. Org. Chem.* **1995**, *60*, 10−11.

(7) Togni, A.; Breutel, C.; Schnyder, A.; Spindler, F.; Landert, H.; Tijani, A. A Novel Easily Accessible Chiral Ferrocenyldiphosphine for Highly Enantioselective Hydrogenation, Allylic Alkylation, and Hydroboration Reactions. *J. Am. Chem. Soc.* **1994**, *116*, 4062−4066.

(8) Priego, J.; García Mancheño, O.; Cabrera, S.; Gómez Arrayás, R.; Llamas, T.; Carretero, J. C. 1-Phosphino-2-Sulfenylferrocenes: Efficient Ligands in Enantioselective Palladium-Catalyzed Allylic Substitutions and Ring Opening of 7-Oxabenzonorbornadienes. *Chem. Commun.* **2002**, *21*, 2512−2513.

(9) (a) Gómez Arrayás, R.; Adrio, J.; Carretero, J. C. Recent Applications of Chiral Ferrocene Ligands in Asymmetric Catalysis. *Angew. Chem., Int. Ed.* **2006**, *45*, 7674−7715. (b) Cunningham, L.; Benson, A.; Guiry, P. J. Recent Developments in the Synthesis and Applications of Chiral Ferrocene Ligands and Organocatalysts in Asymmetric Catalysis. *Org. Biomol. Chem.* **2020**, *18*, 9329−9370.

(10) (a) Deng, W. P.; You, S. L.; Hou, X. L.; Dai, L. X.; Yu, Y. H.; Xia, W.; Sun, J. Importance of Planar Chirality in Chiral Catalysts with Three Chiral Elements: The Role of Planar Chirality in 2′-Substituted 1,1′-P,N-Ferrocene Ligands on the Enantioselectivity in Pd-Catalyzed Allylic Substitution. *J. Am. Chem. Soc.* **2001**, *123*, 6508−6519. (b) Dai, L. X.; Tu, T.; You, S. L.; Deng, W. P.; Hou, X. L. Asymmetric Catalysis with Chiral Ferrocene Ligands. *Acc. Chem. Res.* **2003**, *36*, 659−667.

(11) (a) Sengupta, S.; Shi, X. Recent Advances in Asymmetric Gold Catalysis. *ChemCatChem.* **2010**, *2*, 609−619. (b) Zi, W.; Toste, F. D. Recent advances in enenatioselective gold catalysis. *Chem. Soc. Rev.* **2016**, *45*, 4567−4589. (c) Jiang, J.-J.; Wong, M.-K. Recent Advances in the Development of Chiral Gold Complexes for Catalytic Asymmetric Catalysis. *Chem.—Asian J.* **2021**, *16*, 364−377. (d) Zuccarello, G.; Escofet, I.; Caniparoli, U.; Echavarren, A. M. New Generation Ligand Design for the Gold Catalyzed Asymmetric Activation of Alkynes. *ChemPlusChem.* **2021**, *86*, 1283−1296.

(12) Ito, Y.; Sawamura, M.; Hayashi, T. Catalytic Asymmestric Aldol Reaction: Reaction of Aldehydes with Isocyanoacetate Catalyzed by a Chiral Ferrocenylphosphine-Gold(I) Complex. *J. Am. Chem. Soc.* **1986**, *108*, 6405−6406.

(13) Pérez-Sánchez, J. C.; Pérez Herrera, R.; Gimeno, M. C. Ferrocenyl complexes as efficient catalysts. *Eur. J. Inorg. Chem.* **2022**, DOI: 10.1002/ejic.202101067.

(14) García-Morales, C.; Ranieri, B.; Escofet, I.; López-Suarez, L.; Obradors, C.; Konovalov, A. I.; Echavarren, A. M. Enantioselective Synthesis of Cyclobutenes by Intramolecular [2 + 2] Cycloaddition with Non-C2 Symmetric Digold Catalysts. *J. Am. Chem. Soc.* **2017**, *139*, 13628−13631.

(15) (a) Ferber, B.; Top, S.; Welter, R.; Jaouen, G. A New Efficient Route to Chiral 1,3-Disubstituted Ferrocenes: Application to the Syntheses of (Rp)- And (Sp)-17α-[(3′-Formylferrocenyl) Ethynyl] Estradiol. *Chem.—Eur. J.* **2006**, *12*, 2081−2086. (b) D'Antona, N.; Lambusta, D.; Morrone, R.; Nicolosi, G.; Secundo, F. Biocatalytic Procedure for Obtaining All Four Diastereoisomers of 1-(1-Hydroxyethyl)-3-Ethylferrocene: Synthons for Chiral 1,3-Disubstituted Ferrocenes. *Tetrahedron Asymmetry* **2004**, *15*, 3835−3840. (c) Steurer, M.; Tiedl, K.; Wang, Y.; Weissensteiner, W. Stereoselective Synthesis of Chiral, Non-Racemic 1,2,3-Tri- and 1,3-Disubstituted Ferrocene Derivatives. *Chem. Commun.* **2005**, *39*, 4929−4931. (d) Steurer, M.; Wang, Y.; Mereiter, K.; Weissensteiner, W. Bromide-Mediated Ortho-Deprotonation in the Synthesis of Chiral, Nonracemic Ferrocene Derivatives. *Organometallics* **2007**, *26*, 3850−3859.

(16) Tazi, M.; Hedidi, M.; Erb, W.; Halauko, Y. S.; Ivashkevich, O. A.; Matulis, V. E.; Roisnel, T.; Dorcet, V.; Bentabed-Ababsa, G.; Mongin, F. Fluoro- and Chloroferrocene: From 2- to 3-Substituted Derivatives. *Organometallics* **2018**, *37*, 2207−2211.

(17) Zuccarello, G.; Mayans, J. G.; Escofet, I.; Scharnagel, D.; Kirillova, M. S.; Pérez-Jimeno, A. H.; Calleja, P.; Boothe, J. R.; Echavarren, A. M. Enantioselective Folding of Enynes by Gold(I) Catalysts with a Remote C2-Chiral Element. *J. Am. Chem. Soc.* **2019**, *141*, 11858−11863.

(18) Riant, O.; Argouarch, G.; Guillaneux, D.; Samuel, O.; Kagan, H. B. A Straightforward Asymmetric Synthesis of Enantiopure 1,2-Disubstituted Ferrocenes. *J. Org. Chem.* **1998**, *63*, 3511−3514.

(19) Sasamori, T.; Sakagami, M.; Niwa, M.; Sakai, H.; Furukawa, Y.; Tokitoh, N. Synthesis of a Stable 1,2-Bis(Ferrocenyl) Diphosphene. *Chem. Commun.* **2012**, *48*, 8562−8564.

(20) Falivene, L.; Cao, Z.; Petta, A.; Serra, L.; Poater, A.; Oliva, R.; Scarano, V.; Cavallo, L. Towards the online computer-aided design of catalytic pockets. *Nat. Chem.* **2019**, *11*, 872−879.
(21) Clavier, H.; Nolan, S. P. Percent buried volume for phosphine and N-heterocyclic carbene ligands: steric properties in organometallic chemistry. *Chem. Commun.* **2010**, *46*, 841−861.
(22) Pizarro, J. D.; Molina, F.; Fructos, M. R.; Pérez, P. J. Gold Complexes with ADAP Ligands: Effect of Bulkiness in Catalytic Carbene Transfer Reactions (ADAP = Alkoxydiaminophosphine). *Organometallics* **2020**, *39*, 2553−2559.
(23) Ruch, A. A.; Ellison, M. C.; Nguyen, J. K.; Kong, F.; Handa, S.; Nesterov, V. N.; Slaughter, L. M. Highly Sterically Encumbered Gold Acyclic Diaminocarbene Complexes: Overriding Electronic Control in Regiodivergent Gold Catalysis. *Organometallics* **2021**, *40*, 1416−1433.
(24) For further details, see Supporting Information. A dataset collection of computational results is available in the ioChem-BD repository and can be accessed https://iochem-bd.iciq.es/browse/handle/100/37192: Álvarez-Moreno, M.; De Graaf, C.; Lopez, N.; Maseras, F.; Poblet, J. M.; Bo, C. Managing the Computational Chemistry Big Data Problem: The ioChem-BD Platform. *J. Chem. Inf. Model.* **2015**, *55*, 95−103.
(25) (a) Kang, R.; Chen, H.; Shaik, S.; Yao, J. Assessment of Theoretical Methods for Complexes of Gold(I) and Gold(III) with Unsaturated Aliphatic Hydrocarbon: Which Density Functional Should We Choose? *J. Chem. Theory Comput.* **2011**, *7*, 4002−4011. (b) Ciancaleoni, G.; Rampino, S.; Zuccaccia, D.; Tarantelli, F.; Belanzoni, P.; Belpassi, L. An ab Initio Benchmark and DFT Validation Study on Gold(I)-Catalyzed Hydroamination of Alkynes. *J. Chem. Theory Comput.* **2014**, *10*, 1021−1034.
(26) Escofet, I.; Armengol-Relats, H.; Bruss, H.; Besora, M.; Echavarren, A. M. On the Structure of Intermediates in Enyne Gold(I)-Catalyzed Cyclizations: Formation of *trans*-Fused Bicyclo[5.1.0]octanes as a Case Study. *Chem.—Eur. J.* **2020**, *26*, 15738−15745.
(27) (a) Seguin, T. J.; Wheeler, S. E. Stacking and Electrostatic Interactions Drive the Stereoselectivity of Silylium-Ion Asymmetric Counteranion-Directed Catalysis. *Angew. Chem., Int. Ed.* **2016**, *55*, 15889−15893. (b) Neel, A. J.; Hilton, M. J.; Sigman, M. S.; Toste, F. D. Exploiting non−covalent π interactions for catalyst design. *Nature* **2017**, *543*, 637−646. (c) Toste, F. D.; Sigman, M. S.; Miller, S. J. Pursuit of Noncovalent Interactions for Strategic Site-Selective Catalysis. *Acc. Chem. Res.* **2017**, *50*, 609−615.
(28) (a) Johnson, E. R.; Keinan, S.; Mori-Sanchez, P.; Contreras-Garcia, J.; Cohen, A. J.; Yang, W. Revealing Noncovalent Interactions. *J. Am. Chem. Soc.* **2010**, *132*, 6498−6506. (b) Contreras-Garcia, J.; Johnson, E. R.; Keinan, S.; Chaudret, R.; Piquemal, J. P.; Beratan, D. N.; Yang, W. NCIPLOT: A Program for Plotting Noncovalent Interaction Regions. *J. Chem. Theory Comput.* **2011**, *7*, 625−632.

https://doi.org/10.1021/acscatal.1c05827
ACS Catal. 2022, 12, 3317−3322